Mon. Not. R. Astron. Soc. **398,** 1263–1278 (2009) doi:10.1111/j.1365-2966.2009.15234.x

The ultraviolet spectrum of the gravitationally lensed galaxy 'the Cosmic Horseshoe': a close-up of a star-forming galaxy at $z \sim 2$

Anna M. Quider,[1⋆] Max Pettini,[1] Alice E. Shapley[2] and Charles C. Steidel[3]

[1] *Institute of Astronomy, Madingley Rd, Cambridge CB3 0HA*
[2] *Department of Physics and Astronomy, University of California, Los Angeles, CA 90095-1547, USA*
[3] *California Institute of Technology, Mail Stop 105-24, Pasadena, CA 91125, USA*

Accepted 2009 June 8. Received 2009 June 7; in original form 2009 May 1

ABSTRACT

Taking advantage of strong gravitational lensing, we have recorded the rest-frame ultraviolet (UV) spectrum of the $z = 2.38115$ galaxy 'the Cosmic Horseshoe' (J1148+1930) at higher resolution and signal-to-noise ratio than is currently feasible for unlensed galaxies at $z = 2$–3. With a star formation rate of $\sim$100 $M_\odot$ yr^{-1}, dynamical mass $M_{\rm vir} \simeq 1 \times 10^{10}\,M_\odot$, half-solar metallicity and moderate reddening $E(B-V) = 0.15$, the Cosmic Horseshoe is a good example of the population of galaxies responsible for most of the star formation activity at these redshifts.

From the analysis of stellar spectral features we conclude that a continuous mode of star formation with a Salpeter slope for stars in the mass range 5–100 $M_\odot$ gives a good representation of the UV spectrum, ruling out significant departures from a 'standard' initial mass function. Generally, we find good agreement between the values of metallicity deduced from stellar and nebular tracers. Interstellar absorption is present over a velocity range $\Delta v \simeq 1000$ km s^{-1}, from -800 to $+250$ km s^{-1} relative to the stars and their H II regions, but we still lack a model relating the kinematic structure of the gas to its location within the galaxy. There is evidence to suggest that the outflowing interstellar gas is patchy, covering only $\sim$60 per cent of the UV stellar continuum.

The Lyα line shares many of the characteristics of the so-called Lyα emitters; its double-peaked profile can be reproduced by models of Lyα photons resonantly scattered by an expanding shell of gas and dust, with $\sim$10–15 per cent of the photons escaping the galaxy. Many of the physical properties of the Cosmic Horseshoe are similar to those of the only other galaxy at $z = 2$–3 studied in comparable detail up to now: MS 1512−cB58. The fact that these two galaxies have drastically different Lyα lines may be due simply to orientation effects, or differences in the covering factor of outflowing gas, and cautions against classifying high-z galaxies only on the basis of spectral features, such as Lyα, whose appearance can be affected by a variety of different parameters.

Key words: galaxies: evolution – galaxies: individual: Cosmic Horseshoe – galaxies: starburst – cosmology: observations.

1 INTRODUCTION

In the 13 yr that have elapsed since the term 'Lyman-break galaxy' (or LBG) was coined, samples of galaxies at $z = 2$–4 have increased a thousand fold. Large surveys, selecting galaxies not only via the break at 912 Å (due mostly to intergalactic H I absorption), but also via Lyα emission, a variety of colour criteria and submm emission, have given us a broad view of the galaxy population during the epoch when star formation activity was at its peak in the history of our Universe (see Pettini et al. 2007 for a brief review).

However, typical galaxies at $z \simeq 3$ are faint, with fiducial $\mathcal{R}$-band magnitude $m^*_{\mathcal{R}} = 24.4$ (Steidel et al. 1999; Reddy et al. 2008), so that, even with the most efficient optical and infrared (IR) telescopes and spectrographs currently available, it is only possible to record their spectra with limited resolution and signal-to-noise ratio (S/N). Until the next generation of 30+ m optical/IR telescopes comes into operation, the only strategy at our disposal for studying *in detail*

⋆E-mail: aquider@ast.cam.ac.uk

the internal properties of normal galaxies at these redshifts is to take advantage of fortuitous alignments with foreground mass concentrations (massive galaxies or galaxy clusters) which can provide an order-of-magnitude boost of the flux reaching the Earth through gravitational lensing.

For several years, the archetypal object for this kind of study has been the LBG MS 1512−cB58 (or cB58 for short; Yee et al. 1996). The magnification by a factor of ∼30 (Seitz et al. 1998) provided by an intervening galaxy cluster at $z = 0.37$ brings this L^*, $z = 2.7276$, galaxy within reach of high-resolution spectroscopy from the ground and has made it the target of extensive observations at wavelengths from the visible to the mm range (Pettini et al. 2000, 2002; Teplitz et al. 2000; Baker et al. 2001, 2004; Sawicki 2001; Savaglio, Panagia & Padovani 2002; Siana et al. 2008). These studies provided unprecedented clear views of the interstellar medium, young stars, star formation history, dust, metallicity, kinematics and many other physical properties of a 'typical' LBG at $z \sim 3$.

But how typical is cB58? We know from the work of Shapley et al. (2003) that its ultraviolet (UV) continuum is more reddened, and its interstellar absorption lines are stronger, than in an 'average' LBG. Furthermore, its young age of only 10–20 Myr (Ellingson et al. 1996; Siana et al. 2008) is at the lower end of the wide range of values deduced by fitting the spectral energy distributions of galaxies at $z = 2$–3 (Papovich, Dickinson & Ferguson 2001; Shapley et al. 2001; Erb et al. 2006b), although it is likely that an older stellar population is present too. Clearly, it is important to study in detail several other similarly bright sources and establish the *range* of properties of galaxies at a given cosmic epoch, rather than naively assuming that any particular galaxy is representative of a whole population. Fortunately, the large area of sky surveyed by the Sloan Digital Sky Survey (SDSS) has led to the recent identification of many other examples of highly magnified galaxies (see, for instance, Belokurov et al. 2009; Kubo et al. 2009, and references therein). These and other discoveries have spurred a number of follow-up studies (e.g. Smail et al. 2007; Stark et al. 2008; Finkelstein et al. 2009; Hainline et al. 2009; Yuan & Kewley 2009).

With these new samples of objects it will be possible to make progress on a variety of outstanding questions which cannot be satisfactorily addressed with lower resolution data. In particular

(i) To what extent do different metallicity indicators, based on stellar photospheric lines, wind lines from the most massive stars, interstellar absorption lines and emission lines from H II regions, give consistent answers? This is an important issue, not only to explore the degree of chemical homogeneity of galaxies undergoing rapid star formation, but also to clarify the sources of the systematic offsets between different H II region metallicity calibrators, and possibly bring them into better internal agreement (see, for example, the discussions by Pettini 2006; Kewley & Ellison 2008).

(ii) What do the profiles of the interstellar absorption lines tell us about large-scale outflows in actively star-forming galaxies and about the inflow of gas fuelling star formation? Can we see any evidence of the leakage of hydrogen ionizing photons from the sites of star formation into the intergalactic medium (IGM) which has proved so difficult to detect directly (e.g. Shapley et al. 2006; Iwata et al. 2009) and yet seems to be required by a number of indirect lines of evidence (e.g. Faucher-Giguère et al. 2008)?

(iii) Can we place limits on possible variations of the stellar initial mass function (IMF) at $z = 2$–3? Claims to this effect have certainly been put forward (e.g. Wilkins et al. 2008 and references therein), but the evidence is still controversial (e.g. Reddy & Steidel 2009).

(iv) What are the factors affecting the wide variety of spectral morphologies of the Lyα line, from strong narrow emission to damped absorption (e.g. Mas-Hesse et al. 2003; Verhamme, Schaerer & Maselli 2006), and what can we learn about the relationship of the so-called 'Lyα emitters' to the more general LBG population?

In this paper we address these and other related questions with new observations of the rest-frame UV spectrum of a recently identified highly magnified LBG, named 'the Cosmic Horseshoe' by its discoverers (Belokurov et al. 2007). The paper is organised as follows. In Section 2, we summarize the known properties of the Cosmic Horseshoe, and in Section 3, we provide details of our observations and data reduction. In Section 4, we consider the information provided by the stellar UV spectrum of this galaxy, concerning in particular its systemic redshift, massive star IMF and metallicity of the OB stars. Section 5 deals with the resolved profiles of the interstellar absorption lines, while Sections 6 and 7 focus on the UV nebular emission lines covered by our spectrum, Lyα and C III] λ1909, respectively. In Section 8, we bring these different strands together in the light of the questions raised above. Finally, we summarize our main conclusions in Section 9. Throughout the paper, we adopt a cosmology with $\Omega_M = 0.3$, $\Omega_\Lambda = 0.7$ and $H_0 = 70\,\mathrm{km\,s^{-1}\,Mpc^{-1}}$.

2 THE COSMIC HORSESHOE

The Cosmic Horseshoe, or J1148+1930, is a nearly complete blue Einstein ring of 10-arcsec diameter encircling a red galaxy (Fig. 1; see also http://www.ast.cam.ac.uk/research/cassowary/). Low-resolution spectroscopy by Belokurov et al. (2007) revealed the lens to be a massive luminous red galaxy ($M \sim 6 \times 10^{12}\,\mathrm{M_\odot}$) at $z = 0.444$ and the ring to be the gravitationally lensed image of a star-forming galaxy at $z = 2.379$. From the extent of the ring, Belokurov et al. estimated an approximate magnification factor of ∼35, while the detailed lensing models constructed by Dye et al. (2008) give overall magnification factors of 24 ± 2. Adopting the latter value, and interpolating between the total integrated

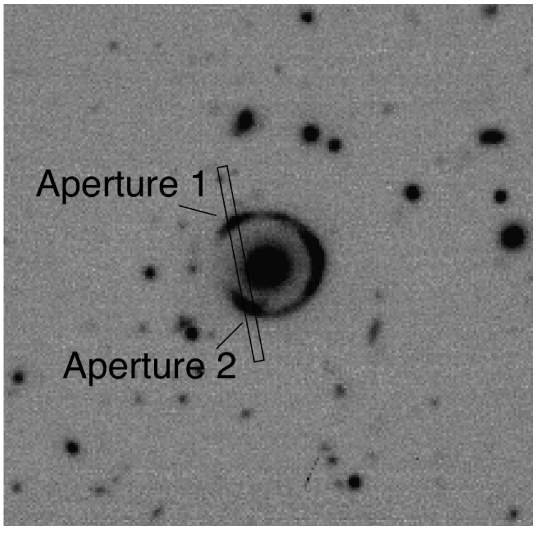

Figure 1. *R*-band image of the Cosmic Horseshoe obtained with Focal Reducer/low dispersion Spectrograph 2 (FORS2) on the Very Large Telescope of the European Southern Observatory (courtesy of L. J. King). North is up and east is to the left. Superposed on the image is the $1.0 \times 20\,\mathrm{arcsec^2}$ entrance slit of ESI used for the observations reported here.

magnitudes of the ring $g = 20.1, i = 19.7$ reported by Belokurov et al. (2007), we deduce a luminosity $L \simeq 2.4L^*$ for the source, relative to $M^*_{\rm AB}$ (1700 Å) $= -21.0$ from the luminosity function of UV-selected $z \simeq 2$ galaxies by Reddy et al. (2008). The image reconstruction in the source plane with the best-fitting lensing model by Dye et al. (2008) shows that the major contributor to this luminosity is a compact source with half-light radius $r_{1/2} \sim 0.3$ arcsec, or ∼2.5 kpc at $z = 2.379$; there is also evidence for a second, fainter, source ∼0.7 arcsec to the north.

We briefly review the information currently available on the lensed galaxy. Its rest-frame UV spectrum is essentially flat in F_ν, reflecting a recent star formation episode and modest reddening [$E(B - V) \simeq 0.1$–0.2; Belokurov et al. 2007], but a more extensive characterization of its stellar population(s) awaits longer wavelength photometry to build-up the spectral energy distribution from the UV to the near-IR (e.g. Shapley et al. 2005; Erb et al. 2006b). Recently, Hainline et al. (2009) reported observations of several rest-frame optical emission lines formed in the H II regions of the Cosmic Horseshoe, from which they were able to measure a number of parameters of interest. The Hα luminosity implies a star formation rate (SFR) of 113 $M_\odot$ yr^{-1}, after correcting for reddening and a lensing magnification factor of 24. The emission line widths indicate a velocity dispersion $\sigma \simeq 65$ km s^{-1} and a corresponding virial mass $M_{\rm vir} \simeq 1.0 \times 10^{10}\,M_\odot$. The oxygen abundance deduced from the ratios of the strongest emission lines is in the range $({\rm O/H})_{\rm H\,II} \simeq 0.5$–$1.5\,({\rm O/H})_\odot$. These parameters are typical of UV-bright galaxies at $z \sim 2$ (Erb et al. 2006a,b,c), although the SFR is at the upper end of the distribution of values found by Erb et al. (2006c). It is of interest now to compare such estimates with those provided by the rest-frame UV spectrum.

3 OBSERVATIONS AND DATA REDUCTION

We observed the Cosmic Horseshoe with the Echellette Spectrograph and Imager (ESI; Sheinis et al. 2000) on the Keck II telescope. The high efficiency, moderately high resolution ($R = 4000$ with a 1-arcsec slit, sampled with 11.4 km s^{-1} pixels) and wide spectral coverage of ESI – from 4000 to 10 000 Å, or 1184 to 2959 Å in the rest frame of the Cosmic Horseshoe – make it highly suitable for an in-depth study of the UV spectrum of this galaxy. The data were collected over two nights (2008 March 6 and 7 UT) in mostly subarcsecond seeing; the total exposure time was 36 100 s, made up of a number of 1800 s or 2000 s long individual integrations. The ESI slit was oriented at sky position angle (PA) $= 10\overset{\circ}{.}8$ east of north, and positioned so as to encompass the two brightest knots in the Einstein ring, as shown in Fig. 1. The northern knot, labelled 'Aperture 1' in the figure, is knot 'A' in the labelling of the features by Belokurov et al. (2007), while 'Aperture 2' corresponds to their knot 'D'. Both knots are due to the same object in the source plane, although 'Aperture 1' may include a small contribution from the fainter component ∼0.7 arcsec to the north of the main source of the ring (Dye et al. 2008). The location of the ESI slit is the same as that of the NIRSPEC observations by Hainline et al. (2009).

The data were processed with standard IRAF tasks. Each individual two-dimensional (2D) ESI spectrum was geometrically corrected (to correct for the spectral curvature of each echellette order), bias-subtracted, flat-fielded and corrected for cosmetic defects and cosmic ray affected pixels. In the next step, all of the images thus processed were co-added into a total 2D frame which was then background subtracted. The background subtraction process included careful modelling of the distribution along the slit of light from the lens, which is clearly visible above the sky at the longer wavelengths of the ESI range. Finally, two 1D spectra were extracted (using optimal extraction algorithms), one for each 'aperture'. The extraction process included merging the 10 echellette orders of ESI into one continuous spectrum, with weighted addition of portions of adjacent orders which overlap in wavelength.

We compared carefully the 1D spectra of Apertures 1 and 2 to look for differences which one may expect to be revealed by the gravitational magnification of any spatial structure in the source, but found none. Neither dividing one spectrum by the other nor subtracting one from the other revealed features more significant than the noise. As discussed in Section 6, this is also the case for the Lyα emission line which (a) has the highest S/N, and (b) is most sensitive to geometrical effects, being resonantly scattered. The only difference between the two apertures is in the total flux: emission line and continuum are uniformly higher by a factor of 1.19 in Aperture 2 than in Aperture 1. Thus, in order to improve the S/N, the two spectra were averaged and the resulting spectrum mapped onto 0.5-Å bins.

This final spectrum has a resolution full width at half-maximum (FWHM) $= 75$ km s^{-1}, sampled with three wavelength bins at 6000 Å, as determined from the widths of narrow emission lines from the Cu–Ar and Hg–Ne–Xe hollow-cathode lamps used for wavelength calibration, whose spectrum was processed in the same way as that of the Horseshoe. From the rms deviation of the data from the mean, we measured an average S/N $\simeq 8$ per 0.5 Å wavelength bin between ∼4000 and ∼7500 Å (∼1200 and ∼2200 Å in the rest frame), with a factor of ∼50 per cent variation in S/N across each echellette order. At the wavelengths of the Lyα emission line the S/N rises to a maximum S/N $= 44$ per 0.5-Å bin.

We attempted to put our spectrum on an absolute flux scale by reference to those of three flux-standard stars recorded during the two nights of observation, but found a scatter of ±20 per cent in the flux calibration among the three stars. Adopting the mean value of the three flux scales, we deduced a mean $\langle f_\nu \rangle = 8.3 \times 10^{-29}$ erg s^{-1} cm^{-2} Hz^{-1} between 4200 and 5485 Å. This wavelength interval corresponds to the FWHM of the transmission curve of the Gunn g filter through which Belokurov et al. (2007) measured $g = 20.1$ (corresponding to $\langle f_\nu \rangle = 3.3 \times 10^{-28}$ erg s^{-1} cm^{-2} Hz^{-1}) for the entire Einstein ring. Thus, if the flux calibration is correct, the ESI slit captured a fraction 0.25 ± 0.05 of the light of the Cosmic Horseshoe, corresponding to an effective magnitude within the two apertures of $g = 21.6 \pm 0.2$.

4 THE STELLAR SPECTRUM

The rest-frame UV spectra of star-forming galaxies are complex blends of interstellar absorption lines, nebular emission lines and absorption/emission lines formed in the atmospheres of OB stars. This wealth of spectral features, properly interpreted, is a rich source of information on the physical properties of the gas and stars in these galaxies. In this section, we consider photospheric absorption lines which have been shown to be useful abundance diagnostics, and P Cygni profiles formed in the expanding atmospheres of the most luminous early-type stars whose strength is also sensitive to the upper end of the IMF.

4.1 The systemic redshift of the Cosmic Horseshoe

The first step in the analysis is the determination of the systemic redshift of the galaxy. While most photospheric features are unresolved blends of multiple lines, a few exceptions allow the redshift of the hot stars to be determined. Within the wavelength range covered by

Table 1. Systemic redshift.

Ion	$\lambda^a_{\rm lab}$ (Å)	$z_{\rm abs}$	Origin
S V	1501.763	2.38107	Stars
N IV	1718.551	2.38119	Stars
C III]	1906.683	2.38103	H II regions
C III]	1908.734	2.38127	H II regions
C III	2297.579	2.38118	Stars
Hα^b	6564.614	2.38123	H II regions

[a] Vacuum wavelengths.
[b] As reported by Hainline et al. (2009).

our data, we identified the following unblended photospheric absorption lines: S V λ1501.763, N IV λ1718.551 and C III λ2297.579 [$\lambda_{\rm air} = 2296.871$ – all three vacuum wavelengths from the National Institute of Standards and Technology (NIST) database available at http://physics.nist.gov/PhysRefData/ASD/].

The redshifts of these three lines are in good mutual agreement (see Table 1), and define an average $z_{\rm stars} = 2.38115 \pm 0.00006$. The 1σ error corresponds to an uncertainty of $\pm 5\,{\rm km\,s^{-1}}$, or 1/5 of a wavelength bin in our final spectrum. Also included in Table 1 are values of $z_{\rm H\,II}$ from the C III] λλ1906.683, 1908.734 doublet lines which are resolved in our ESI spectrum (see Section 7), and from Hα measured from the NIRSPEC spectrum of Hainline et al. (2009). The mean $z_{\rm C\,III]} = 2.38115 \pm 0.00012$ is in excellent agreement with $z_{\rm stars}$; $z_{\rm H\alpha}$ differs by only $7\,{\rm km\,s^{-1}}$ which may include a small systematic offset between the wavelength calibrations of the ESI and NIRSPEC spectra. Thus, we conclude that the systemic redshift of the Cosmic Horseshoe is $z_{\rm sys} = 2.38115$ and we adopt this value throughout the paper.

4.2 Photospheric lines

In this and the following subsection, we analyse photospheric and wind lines in the spectrum of the Cosmic Horseshoe by comparing our data with model spectra computed with the population synthesis code STARBURST99 which couples libraries of either empirical (Leitherer et al. 1999, 2001) or theoretical (Rix et al. 2004) UV OB stellar spectra with stellar evolutionary tracks. The input set of parameters to STARBURST99 can be adjusted to simulate a variety of star formation histories, ages, IMF parameters and metallicities so as to determine the combination that best fits the observations under scrutiny.

In the absence of more detailed information on the previous history of star formation in the Cosmic Horseshoe, we shall adopt the simplest case of continuous star formation – with a Salpeter slope of the upper end of the IMF – which has been proceeding at a steady rate (as opposed to a declining rate, or a series of bursts) for 100 Myr (this being a safe lower limit beyond which the spectrum no longer changes with time because the stars that contribute to the UV light are born and die at the same rate). While this scenario is undoubtedly an oversimplification, it may not be too different from reality when considering the spectrum of a whole galaxy, rather than individual regions of star formation. An age of more than 100 Myr is typical of most $z = 2$ UV-bright galaxies in the 'BX' sample of Erb et al. (2006b) and seems plausible given the near-solar metallicity of the H II regions of the Horseshoe (Hainline et al. 2009).

Leitherer et al. (2001) and Rix et al. (2004) pointed out the existence of some blends of UV photospheric lines whose strengths, under the above assumptions, depend on metallicity (see also Halliday et al. 2008). The '1425' index of Rix et al. (2004) measures the equivalent width of a blend of Si III λ1417, C III λ1427 and Fe V λ1430 absorption lines spanning the wavelength interval 1415–1435 Å; at longer wavelengths, the '1978' index measures the strengths of several Fe III absorption lines from B stars between 1935 and 2020 Å. Both indices stabilize after ∼50 Myr from the onset of star formation, and increase monotonically with metallicity. In the left-hand portion of Fig. 2, we compare the ESI spectrum of the Cosmic Horseshoe with the model spectra of Rix et al. (2004) for five values of metallicity, from 1/20 of solar to twice solar, in the regions of the 1425 and 1978 indices. For this comparison, we smoothed our spectrum to the 2.5-Å resolution of the Rix et al. models, and normalized it using the pseudo-continuum windows suggested by those authors. Thus, the observed and model spectra should be directly comparable.

Fig. 2 shows a generally good agreement in the detailed features of the synthetic and real spectra in the two wavelength regions considered here, attesting to the sophistication reached by current hot-star atmosphere and stellar population synthesis models. Referring to the 1425-Å region (left-most panel in Fig. 2), it can be seen that the strength of the photospheric lines in this region of the Cosmic Horseshoe spectrum is intermediate between those computed with metallicities $Z = 0.4$ and $1.0\,{\rm Z_\odot}$, respectively. Using the relationship between metallicity and the 1425 index proposed by Rix et al. (2004):

$$\log(Z/{\rm Z_\odot}) = A\,{\rm EW}(1425) + B, \qquad (1)$$

with $A = 1.14$ and $B = -1.75$ appropriate to the value EW (1425) = 0.95 Å we measure here, we derive $Z_{\rm OBstars} = 0.5\,{\rm Z_\odot}$.

Qualitatively, the observed spectrum seems to be intermediate between the 0.4 solar and solar metallicity cases in the 1978 region too (see middle panel of Fig. 2). However, there appears to be excess absorption between 1960 and 1980 Å over that expected from the models for *any* metallicity; the presence of these additional features does not allow us to deduce a value of $Z_{\rm Bstars}$ from EW(1978) using the Rix et al. (2004) calibration of this index. We considered the possibilities that the excess absorption may be noise, or an intervening absorption system unrelated to the Cosmic Horseshoe, but could find no evidence to support either interpretation. It also seems unlikely that the excess is due to a different mix of stellar spectral types or chemical elements, since all of the photospheric absorption in this region is thought to be due to Fe III lines, and the rest of the spectral features between 1920 and 2025 Å match the data well. No such discrepancies were found by Rix et al. (2004) in the two galaxies they considered (MS 1512−cB58 and Q1307−BM1163, the latter at $z = 1.411$), nor by Halliday et al. (2008) in their composite spectrum of $z \sim 2$ galaxies. However, the cases where these photospheric indices have been measured are still very few, and it is important to continue to look critically at the match between model and real spectra as more data of suitable quality become available.

4.3 Wind lines

The model spectra by Rix et al. (2004) show that the spectral features most sensitive to metallicity are the P Cygni lines formed in the expanding winds of the most luminous OB stars whose mass-loss rates are thought to be lower at lower metallicities (e.g. Kudritzki & Puls 2000). Among the P Cygni lines covered by our spectrum, the C IV λλ1548.204, 1550.781 (unresolved) doublet is the strongest. Referring to the right-most panel in Fig. 2, we find that its strength in the Cosmic Horseshoe is intermediate between those of the models with metallicities $Z = 0.2$ and $0.4\,{\rm Z_\odot}$. However, as emphasized

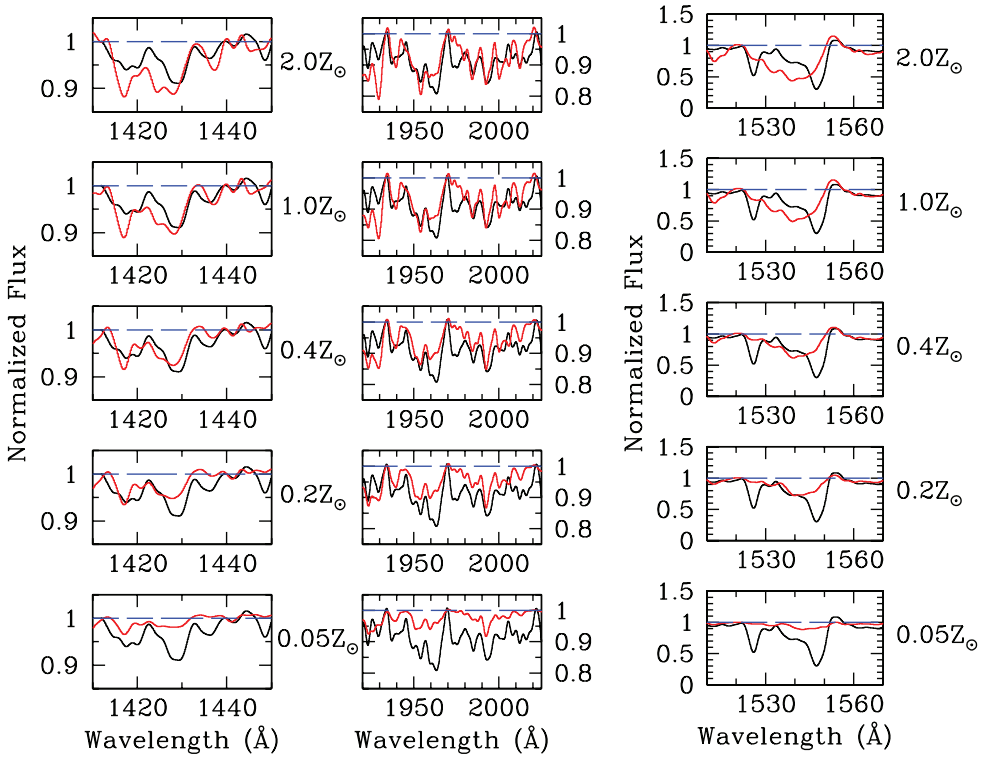

Figure 2. Left-hand pair of panels: portions of the UV spectrum of the Cosmic Horseshoe (black) in the regions encompassing the 1425 and 1978 indices compared with model spectra (red) from the work by Rix et al. (2004) for five different metallicities, as indicated. The ESI spectrum has been smoothed to the 2.5 Å resolution of the model spectra. See text for further details of the models. Right-hand panel: comparison of the Rix et al. models with the smoothed and normalized spectrum of the Cosmic Horseshoe in the region of the C IV λλ1548.204, 1550.781 doublet. This region also includes C IV and Si II λ1526.7070 *interstellar* absorption which is unaccounted for in the Rix et al. models. Note the difference in the *y*-axis scales between the C IV panels and those for the weaker photospheric 1425 and 1978 features to the left.

by Crowther et al. (2006), the interpretation of this feature is complicated by its blending with interstellar C IV (and to a lesser extent Si II λ1526.7070) absorption, at least at the coarse resolution of most spectra of distant galaxies. Similar problems affect the generally weaker Si IV λλ1393.7602, 1402.7729 and N V λλ1238.821, 1242.804 wind lines.

At the high resolution of our ESI spectrum, interstellar and stellar components are easily separated, as can be appreciated from Fig. 3. The top panel compares the observed spectrum of the Cosmic Horseshoe in the C IV region with those generated by STARBURST99 now using libraries of *empirical* stellar spectra, assembled from UV observations of stars in either the Galaxy or the Magellanic Clouds. Both models are for 100 Myr old continuous star formation with Salpeter IMF. Apart from the narrow interstellar Si II λ1526.7070 and C IV λλ1548.204, 1550.781 absorption lines, which are stronger in the distant galaxy than in the spectra of the stars that make up the STARBURST99 libraries, the agreement between models and observations is clearly very good. The broad blue absorption wing of the P Cygni profile reaches similar terminal velocities in the models and the data, and its depth is roughly intermediate between those of the Galactic and Magellanic Clouds models. The latter library of stellar spectra was built-up by Leitherer et al. (2001) with *Hubble Space Telescope* (*HST*) observations of stars in *both* the Large and Small Magellanic Clouds (LMC/SMC) and may thus correspond to an approximate metallicity $Z_{\rm MC} \sim 0.4\,{\rm Z}_{\odot}$, given that in the LMC $({\rm O/H}) \simeq 0.5\,({\rm O/H})_{\odot}$ and in the SMC $({\rm O/H}) \simeq 0.25\,({\rm O/H})_{\odot}$ (e.g. Pagel 2003). By linearly interpolating between the Galactic and LMC models and minimizing the difference from the observed spectrum, we find $Z_{\rm Ostars} \approx 0.6\,{\rm Z}_{\odot}$, in good agreement with $Z_{\rm OBstars} = 0.5\,{\rm Z}_{\odot}$ deduced above from consideration of the 1425 photospheric index.

It is interesting that both Galactic and Magellanic Clouds models seem to *underpredict* the emission component of the P Cygni profile. However, the narrow emission feature centred near 1551.6 Å may be partly of nebular origin (Leitherer, Calzetti, & Martins 2002). Similarly, the narrow emission centred near 1533.7 Å is probably nebular Si II* λ1533.4312; both features are missing from the synthetic spectra which were designed to reproduce only the stellar component of the galaxy spectrum. The superposition of P Cygni broad emission/absorption, photospheric broad absorption, narrow interstellar absorption and narrow nebular emission attests to the complex nature of this portion of the UV spectrum of star-forming galaxies.

In the lower panel of Fig. 3 we compare the ESI spectra of MS 1512−cB58 (from Pettini et al. 2002) and the Cosmic Horseshoe in the wavelength region 1500–1570 Å. There is a startling similarity in this spectral region between these two galaxies which are at different redshifts (cB58 is at $z_{\rm stars} = 2.7276$) and were selected randomly, only by virtue of the fact that they are highly lensed as seen from the Earth (although they are both more luminous than the 'average' galaxy at these redshifts, even after correcting for the lensing magnifications). Presumably, not only the chemical abundances, but also the young stellar populations of these two galaxies are remarkably similar. Only the interstellar absorption lines are different, with those in cB58 apparently stronger than in the Cosmic Horseshoe (but see the discussion in Section 5).

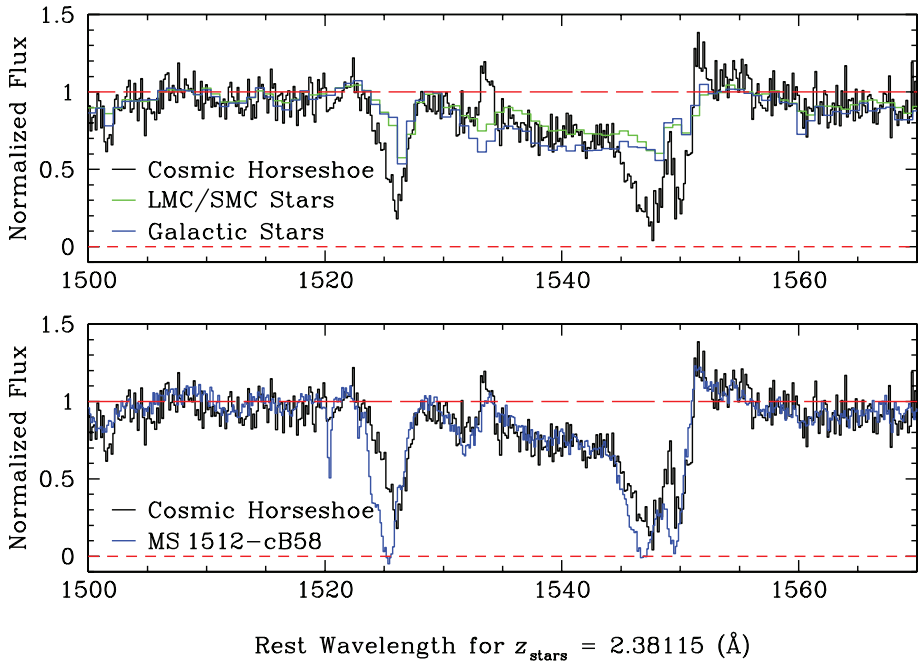

Figure 3. Upper panel: comparison between the ESI spectrum of the Cosmic Horseshoe in the region encompassing the C IV line and model spectra computed with STARBURST99 and empirical libraries of Galactic and Magellanic Clouds stars, as indicated. The model spectra were generated assuming a 100 Myr old continuous star formation episode with a Salpeter IMF. Lower panel: the stellar spectra of the Cosmic Horseshoe and of MS 1512−cB58 are remarkably similar in the wavelength region shown. The ESI spectrum of cB58 is reproduced from Pettini et al. (2002), and has been reduced to its rest wavelengths at z_{stars} = 2.7276.

The P Cygni component of the C IV complex is due to the most massive (and luminous) O stars, which drive the strongest winds. On the other hand, a wider range of stellar spectral types, including all stars with masses greater than about 5 $M_\odot$, is thought to make up the integrated continuum light near 1550 Å (e.g. Rix et al. 2004). Thus, the contrast of the P Cygni features relative to the continuum is sensitive not only to metallicity, but also to the slope and upper end cut-off of the IMF, as well as to more subtle effects, such as differential dust extinction among stars at the upper end of the IMF (the most massive and short-lived stars may in principle be more reddened than longer lived ones – Leitherer, Calzetti & Martins 2002), and the relative proportions of OB stars in star clusters and in the field (Chandar et al. 2005). Pettini et al. (2000) showed how even relatively minor changes to the IMF slope (or alternatively the upper mass cut-off) result in noticeable alterations to the integrated spectrum of a star-forming galaxy in the C IV region. On that basis, those authors concluded that a standard Salpeter IMF extending to $M_{up} > 50\,M_\odot$ provides the best match to the spectrum of cB58, without the need to invoke a different IMF at high redshift, as claimed by some. Clearly, the same conclusion applies here to the massive stellar population in the Cosmic Horseshoe. More generally, the similarity evident in the lower panel of Fig. 3 suggests that the minor effects discussed above (differential dust extinction and the balance between cluster and field stars) presumably average out in at least a subset of star-forming galaxies at $z = 2$–3, when their integrated spectra are considered.

Summarizing the conclusions of this section, we find that the metallicity of the early-type stars in the Cosmic Horseshoe is approximately half-solar, from consideration of photospheric and wind absorption lines. A continuous mode of star formation with a Salpeter slope for stars more massive than 5 $M_\odot$ gives a good representation of the UV spectrum. The 1978 index introduced by Rix et al. (2004) appears to be contaminated by additional features of uncertain origin in the spectrum of the Horseshoe. The C IV region is a complex blend of stellar, interstellar and nebular features, but the stellar component in the Cosmic Horseshoe is surprisingly similar to that in cB58, the only other high-redshift star-forming galaxy studied in comparable detail so far. This may of course be a coincidence, but it may also point to the fact that many of the parameters which can affect the appearance of this spectral region average out to a large extent in the integrated UV spectrum of a whole galaxy.

5 THE INTERSTELLAR SPECTRUM

5.1 Kinematics of the absorbing gas

In the wavelength interval from 1200 to 2600 Å, we identified 21 interstellar absorption lines from six chemical elements in a variety of ionization stages, from O I to C IV. Relevant measurements are collected in Table 2, while Fig. 4 shows selected transitions chosen to illustrate the range of elements and ion stages covered. The interstellar lines in the Cosmic Horseshoe are broad, with absorption extending smoothly from −800 to +250 km s^{-1} with respect to $z_{sys} = z_{stars} = 2.38115$. Within the limits of the noise, we find no convincing differences between the profiles of different ions, although the maximum velocities measured depend on the strength of the transition, as is the case in local starbursts (e.g. Grimes et al. 2009). The values of z_{abs} listed in column 4 of Table 2 are those derived from the centroids of the lines (that is, the mean wavelength of the line weighted by the absorption in each wavelength bin); their mean value is $\langle z \rangle = 2.3788 \pm 0.0009$ which corresponds to a velocity offset $\Delta v = -208$ km s^{-1} with respect to the stars. We also measured the redshift at the peak optical depth in the most clearly

Table 2. Interstellar absorption lines.

Ion	$\lambda^a_{\rm lab}$ (Å)	f^a	$z_{\rm abs}$	$W^b{}_0$ (Å)	σ^b (Å)	Comments
C II	1334.5323	0.1278	2.3786	1.62	0.16	Blended with C II* λ 1335.6627
C IV	1548.204	0.1899	2.3783	2.36	0.08	Blended with stellar C IV λ1549.1; W_0 measured from −800 to +100 km s^{-1}
	1550.781	0.09475	2.3798	0.85	0.04	Blended with stellar C IV λ1549.1; W_0 measured from −250 to +60 km s^{-1}
O I	1302.1685	0.04887	2.3791	0.90	0.09	W_0 measured from −800 to +100 km s^{-1}
Al II	1670.7886	1.74	2.3779	1.48	0.07	
Al III	1854.7184	0.559	2.3792	0.93	0.10	
	1862.7910	0.278	2.3782	0.61	0.13	
Si II	1260.4221	1.18	2.3778	1.71	0.18	Blended with S II λ1259.519
	1304.3702	0.0863	2.3792	0.71	0.06	W_0 measured from −400 to +25 km s^{-1}
	1526.7070	0.133	2.3788	1.81	0.06	
	1808.0129	0.00208	2.3778	0.40	0.08	
Si IV	1393.7602	0.513	2.3795	1.36	0.09	
	1402.7729	0.254	2.3791	1.13	0.08	
Fe II	1608.4511	0.0577	2.3774	0.51	0.12	
	2344.2139	0.114	2.3807	0.40	0.23	
	2374.4612	0.0313	2.3795	1.47	0.23	
	2382.7652	0.320	2.3767	1.25	0.18	W_0 measured from −700 to +250 km s^{-1}
	2586.6500	0.0691	2.3791	1.85	0.13	
	2600.1729	0.239	2.3793	2.25	0.28	
Ni II	1317.217	0.0571	2.3786	0.12	0.05	W_0 measured from −350 to −80 km s^{-1}
	1741.5531	0.0427	2.3799	0.14	0.05	W_0 measured from −180 to −20 km s^{-1}

[a]Vacuum wavelength and f values are from Morton (2003) with updates by Jenkins & Tripp (2006).
[b]Rest-frame equivalent width and associated error measured over the velocity range −800 to +250 km s^{-1} with respect to $z_{\rm stars}$, unless otherwise noted.

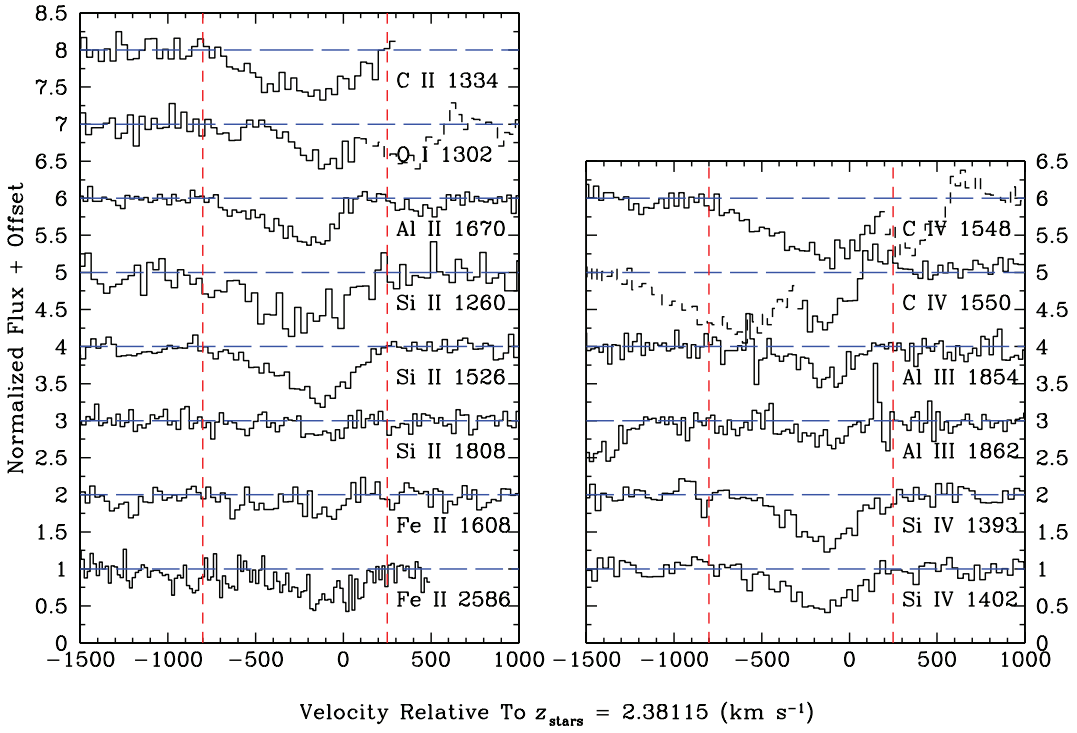

Figure 4. Normalized profiles of selected interstellar absorption lines. Left-hand panel: transitions of ions which are the dominant species of the corresponding elements in H I regions. Right-hand panel: higher ionization stages. In both panels the vertical red dash lines indicate the velocity range over which the values of equivalent width listed in Table 2 were generally measured.

defined line profiles and found a mean $z_{\rm ISM} = 2.3795 \pm 0.0002$ ($\Delta v = -146$ km s^{-1}).

This net blueshift of the interstellar lines is a common feature of star-forming galaxies at low (e.g. Heckman et al. 2000; Martin 2005) as well as high (e.g. Pettini et al. 2001; Shapley et al. 2003; Steidel et al. 2004; Vanzella et al. 2009) redshifts. It is generally interpreted as empirical evidence for the existence of large-scale outflows of the interstellar medium driven by the kinetic energy deposited by supernovae and the winds of massive stars. The values of Δv we deduce here, irrespective of whether one considers the mean redshift of the line centroids or of the gas with the highest optical depth, are typical of $z = 3$ galaxies for which Shapley et al. (2003) derive

a mean $\langle \Delta v \rangle = -150 \pm 60\,\mathrm{km\,s^{-1}}$. Similarly, the widths of the strongest lines (FWHM $\simeq$ 400–600 $\mathrm{km\,s^{-1}}$) are within the range $\langle \mathrm{FWHM} \rangle = 575 \pm 150\,\mathrm{km\,s^{-1}}$ measured by Shapley et al. (2003) from their composite spectrum of 811 LBGs.

Although with the higher resolution of our data (compared to that normally employed to record the spectra of unlensed $z = 2$–3 galaxies) the interstellar lines are fully resolved, we are still unable to recognize clear clues in the line profiles as to the location of the absorbing gas. The profiles are smooth and relatively featureless, and we see no trends between, for example, velocity and degree of ionization, which could be used to construct a kinematical model. While the blueshifted absorption is presumably due to outflowing material, the location and nature of the gas moving at *positive* velocities relative to the stars remain unexplained. It is interesting to note that the absorption lines in the ESI spectrum of MS 1512−cB58 analysed by Pettini et al. (2002) also extend over the same velocity range, from ~ -800 to $\sim +250\,\mathrm{km\,s^{-1}}$ relative to the systemic redshift of the stars, although in cB58 the gas with the highest optical depth is moving at a higher velocity $\Delta v = -255\,\mathrm{km\,s^{-1}}$. The two galaxies have similar SFRs, SFRs $\approx 50\,\mathrm{M_\odot\,yr^{-1}}$, as estimated from their UV continua (see Section 6.3). Overall, the profiles of the interstellar absorption lines from the first ions appear smoother in the Horseshoe than in cB58, but the lower S/N of the present data makes it more difficult to recognize distinct velocity components than is the case in cB58.

5.2 Partial coverage and column densities

One noticeable difference between the Cosmic Horseshoe and cB58 is in the optical depth of the interstellar absorption lines (see Fig. 3). Whereas in cB58 the strongest interstellar lines have saturated cores of zero residual intensity (at the spectral resolution of ESI – see figs 1 and 2 of Pettini et al. 2002), the same transitions never seem to reach below an optical depth $\tau \sim 1$ in the Cosmic Horseshoe, as can be appreciated from inspection of Fig. 4.

One possibility is that the column densities of even the most abundant ions are genuinely lower in the Horseshoe compared to cB58. An alternative explanation is that the interstellar gas does not completely cover the early-type stars producing the UV continuum against which the absorption is seen. The latter interpretation is not unlikely in general – given the composite nature of the UV spectra of star-forming galaxies which are the superposition of hundreds of thousands of individual stellar spectra – and is suggested by the similarity in the residual intensity in the cores of all the strongest absorption lines in Fig. 4.

We can assess quantitatively the partial coverage hypothesis using the apparent optical depth method of Savage & Sembach (1991). If the absorption lines are resolved, as seems to be the case here, the column density of an ion in each velocity bin, $N_\mathrm{a}(v)$ [in units $\mathrm{cm^{-2}\,(km\,s^{-1})^{-1}}$], can be deduced directly from the optical depth in each velocity bin,

$$\tau_\mathrm{a}(v) = -\ln\left[I_\mathrm{obs}(v)/I_0(v)\right], \tag{2}$$

from the relation

$$N_\mathrm{a}(v) = 3.768 \times 10^{14}\,\frac{\tau_\mathrm{a}(v)}{f\lambda}, \tag{3}$$

where f measures the strength of the transition at wavelength λ (Å), and I_obs and I_0 denote the relative intensities in the line and in the continuum, respectively. If multiple absorption lines arising from the same ground state of an ion but with different values of the product $f\lambda$ are available, partial coverage would manifest itself as a mismatch between the values of column density deduced from each transition, the lines with smaller values of $f\lambda$ giving systematically higher values of $N_\mathrm{a}(v)$.

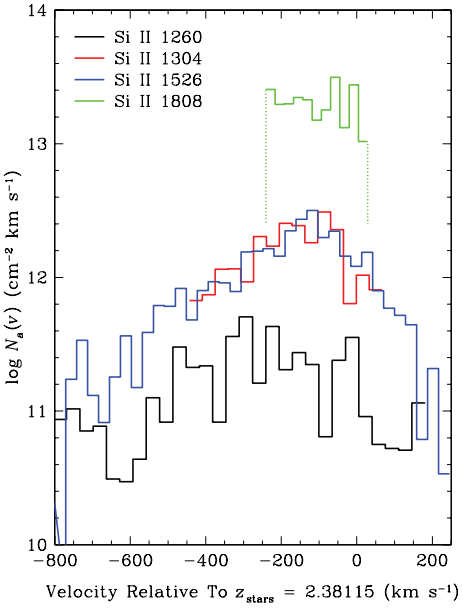

Figure 5. When analysed with the apparent optical depth method, the four Si II transitions recorded in our ESI spectrum of the Cosmic Horseshoe yield values of column density which differ systematically, in the sense expected if the interstellar gas does not completely cover the stellar UV continuum (see Section 5.2 for further details).

Among the ions covered by the ESI spectrum of the Horseshoe, Si II is the one best suited to this analysis, with four transitions spanning a range of ∼400 in $f\lambda$ (see Table 2) and falling at wavelengths where the S/N of the data is highest. As can be seen from Fig. 5, the run of $N_\mathrm{a}(v)$ versus v for the four Si II lines does indeed show the systematic differences expected if the absorbing gas does not completely cover the background stellar continuum. In the line core, the apparent optical depth of the weakest absorption line, Si II λ1808.0129, implies values of column density *two orders of magnitude* higher than those deduced from the strongest transition, Si II λ1260.4221. The profiles of Si II λ1304.3702 and λ1526.7070, with very similar values of $f\lambda$ intermediate between those of the other two lines, indicate that partial coverage extends well beyond the line cores and probably applies to the full velocity range spanned by the absorption.

We also cover several Fe II transitions (see Table 2), but their $f\lambda$ values range over a factor of only ∼10 and most of them are redshifted to far-red wavelengths, where the S/N of our data is lower. Nevertheless, the profiles of the Fe II lines are consistent with the conclusions drawn from Fig. 5, in showing a systematic trend of increasing $N_\mathrm{a}(v)$ with decreasing $f\lambda$. Turning to the high ionization lines in the right-hand panel of Fig. 4, we found that the weaker member of the Si IV doublet, λ1402.7729, also gives systematically higher values of $N_\mathrm{a}(v)$ than λ1393.7602, even though the $f\lambda$ values of the two lines differ by only a factor of 2, while the evidence is less clear-cut in the case of the Al III doublet which is recorded at lower S/N. The C IV lines are difficult to interpret in this context because they are blended with each other and with the stellar P Cygni profile, as discussed above (Section 4.3).

Given our lack of knowledge of the relative configuration of interstellar gas and stars, it is quite possible, or even likely (e.g. Martin & Bouché 2009), that the covering factor varies with velocity and

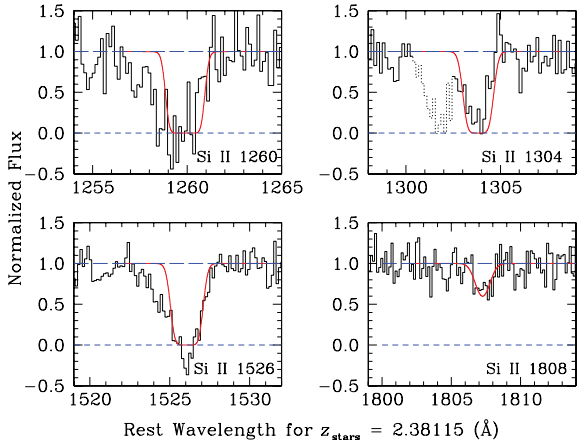

Figure 6. Black histograms: normalized profiles of the four Si II absorption lines after subtracting 40 per cent of the continuum level, under the assumption that the gas only covers 60 per cent of the stellar light. Red continuous lines: theoretical absorption line profiles generated with the values of N(Si II) and velocity dispersion parameter b implied by the weakest transition, λ1808.0129, which is unsaturated. The absorption line shown by the short-dash histogram in the top right-hand panel is O I λ1302.1685.

degree of ionization of the gas. However, the S/N of our data is insufficient to establish the magnitude of such variations. Instead, we adopted the simplest assumption that 'one size fits all' and corrected the absorption line profiles by re-adjusting the zero level by the same fractional amount of the continuum at all wavelengths. Inspection of the spectrum shows that even the strongest absorption lines, which are normally saturated in the spectra of Galactic stars and of nearby starbursts, all seem to have a minimum residual intensity $I_\lambda/I_0 \sim 0.4$ (see Fig. 4). With the simplistic assumption that the interstellar gas only covers 60 per cent of the stellar light, and that the remaining 40 per cent of the UV continuum sees no absorption in our direction, the adjusted profiles of the four Si II lines become internally consistent, as shown in Fig. 6.

Specifically, after subtracting 40 per cent of the stellar continuum and renormalizing the line profiles, we deduced the column density of Si II, $\log N(\mathrm{Si\,II})/\mathrm{cm}^{-2} = 16.00$, by integrating equation (3) over the velocity range spanned by the weakest Si II line, λ1808.0129, which is unsaturated even after the re-adjustment of the zero level. We then used the absorption line fitting software XVOIGT (Mar & Bailey 1995) to fit the profile of Si II λ1808.0129 with this column density and deduced the value of the velocity dispersion parameter, $b = 105\,\mathrm{km\,s}^{-1}$, which best reproduces the width of this line. In the next step, we used this pair of values of N(Si II) and b to generate XVOIGT profiles of the other three Si II absorption lines. As can be seen from Fig. 6, these computed profiles provide satisfactory fits to the main absorption component of the three stronger Si II transitions, given the noise in the data. (We have not attempted to fit the blue wing of the three lines because this absorption is too weak to be detected in Si II λ1808.0129, but its contribution to the value of N_{TOT}(Si II) is only a small fraction of the total, unless the covering factor of the high-velocity gas is much smaller than 60 per cent.)

Table 3 lists the values of ion column density deduced by integrating equation (3) over the velocities spanned by those absorption lines that remain unsaturated after the 40 per cent adjustment of the zero level. Errors in the column density, δN, were determined by adding/subtracting the 1σ error spectrum to/from the line profiles and recalculating the column density; in cases where the addition of the noise spectrum results in the line becoming saturated no corresponding error is given in Table 3. Again, we see from the table that there is good internal agreement between the values of N implied by different transitions of the same ion, after correcting for the 40 per cent unabsorbed stellar continuum.

Table 3. Ion column densities.

Ion	λ_{lab} (Å)	f	$\log N/\mathrm{cm}^{-2}$	$\log \delta N/\mathrm{cm}^{-2}$
Al III	1854.7184	0.559	14.22	−0.06, ...
	1862.7910	0.278	14.26	−0.07, +0.14
Si II	1808.0129	0.00208	16.00	−0.06, +0.07
Si IV	1402.7729	0.254	14.92	−0.06, ...
Fe II	1608.4511	0.0577	14.94	−0.10, +0.11
	2586.6500	0.0691	15.12	−0.06, ...
Ni II	1317.217	0.0571	14.22	−0.24, +0.20
	1741.5531	0.0427	14.40	−0.21, +0.19

The interstellar column densities of the first ions in the Cosmic Horseshoe are surprisingly similar to those measured in cB58 by Pettini et al. (2002). For the transitions in common between the two studies, we have $\log N/\mathrm{cm}^{-2}$ (Horseshoe/cB58) = 16.00/15.99 for Si II λ1808.0129; 14.94/15.17 for Fe II λ1608.4511; 14.22/14.32 for Ni II λ1317.217 and 14.40/≤ 14.45 for Ni II λ1741.5531. Although the metallicities reached by the two galaxies are similar, as discussed above (Section 4), there was no reason to expect that the column densities of interstellar gas entrained by the outflows – nor the ionization of this gas – should be so similar. Furthermore, even the ratios of elements that are depleted onto dust by different degrees, or are synthesised by stars of different masses, are similar between these two galaxies. Thus, the iron-peak and easily depleted elements Fe and Ni are underabundant (in their first ions) compared with the undepleted alpha-capture element Si by about one order of magnitude, as is the case in cB58 (see fig. 8 of Pettini et al. 2002). All of this may just be a coincidence, of course, or may point to a more fundamental uniformity in the conditions of the gas outflowing from high-redshift star-forming galaxies, or at least a subset of such galaxies.

Given the similarity in the column densities of the first ions and in the metallicity of the two galaxies, it follows that we also expect similar values of the column density of hydrogen N(H). Indeed, if the majority of the first ions arises from H I regions, we can deduce values of N(H I) from the column densities in Table 3 and the assumption that $Z_{\mathrm{ISM}} = Z_{\mathrm{OBstars}} = 0.5\,Z_\odot$. This leads to $\log N(\mathrm{H\,I})/\mathrm{cm}^{-2} = 20.79$ using Si II as the reference ion, indeed very close to $\log N(\mathrm{H\,I})/\mathrm{cm}^{-2} = 20.85$ deduced by Pettini et al. (2002) from the damped profile of the Lyα line in cB58. As we shall see in a moment, however, there are striking differences between the profiles of the Lyα line observed in the two galaxies. Whereas in the case of cB58 we see a clear damped absorption profile with a weak superposed emission component, Lyα is in emission in the Cosmic Horseshoe.

6 THE LYMAN α LINE

6.1 Lyman α line morphology

The top panel of Fig. 7 shows the spectral region encompassing the Lyα line in the Cosmic Horseshoe, plotted in arbitrary flux-density units versus velocity relative to the systemic redshift of the galaxy. We interpret the complex morphology as consisting of two main emission components: a narrow, symmetric component which is barely resolved (FWHM $\lesssim 50\,\mathrm{km\,s}^{-1}$ after deconvolution with

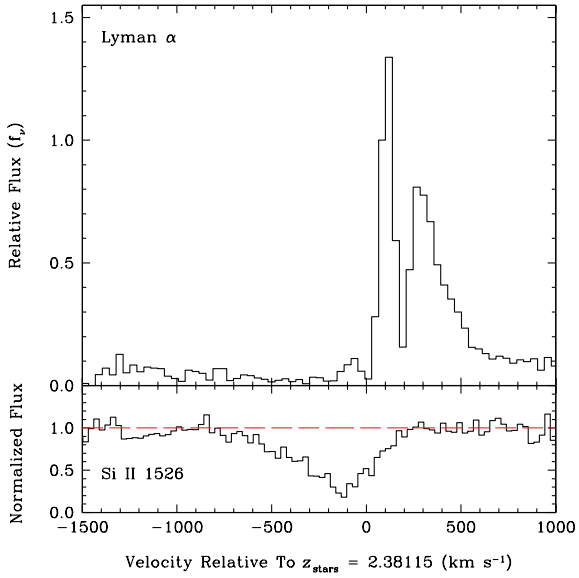

Figure 7. Lyα emission and Si II absorption lines plotted on a common velocity scale. The former mirrors the latter in velocity space.

the ESI spectral resolution of FWHM = 75 km s^{-1}) centred at $v = +115$ km s^{-1}, and a broader, asymmetric component which peaks at $v = +275$ km s^{-1} but extends to $v \simeq +700$ km s^{-1}. The first, narrow component has a peak flux ∼1.5 times higher than that of the second. There may be a third, weak component at negative velocities, centred near $v \sim -80$ km s^{-1}, but its identification is uncertain, given the blending with absorption from the Lyα forest. The total flux in the line, without correcting for gravitational lensing and reddening (these corrections will be applied later – see Section 6.3) is $F(\mathrm{Ly}\alpha) = (4.5 \pm 0.2) \times 10^{-16}$ erg s^{-1} cm^{-2} where the error reflects both the random noise in the data and the uncertainty in the stellar continuum (measured redward of Lyα), combined in quadrature. In our assumed cosmology, the measured flux corresponds to a Lyα luminosity $L(\mathrm{Ly}\alpha) = (2.0 \pm 0.1) \times 10^{43}$ erg s^{-1}. The line equivalent width is $W_0(\mathrm{Ly}\alpha) = (11 \pm 0.2 \pm 2.5)$ Å, (switching sign convention, compared to Table 2, to indicate equivalent widths of emission lines as positive and those of absorption lines as negative); here we have quoted separately the random and systematic errors, respectively, to emphasize that the main uncertainty in the value of $W_0(\mathrm{Ly}\alpha)$ arises from the placement of the underlying stellar continuum. Although the net profile is in emission, the value of $W_0(\mathrm{Ly}\alpha)$ we measure is below the threshold $W_0(\mathrm{Ly}\alpha) \geq 20$ Å generally adopted to define the so-called Lyα emitters (e.g. Hu, Cowie & McMahon 1998; Rhoads et al. 2000; Shapley et al. 2003). Nevertheless, the profile exhibits the broad characteristics that are typical of Lyα emission from high-z galaxies: an abrupt blue edge and an extended red wing (e.g. Tapken et al. 2007); with the high resolution and S/N of our data we can now examine its characteristics in greater detail than is normally possible.

6.2 Comparison to radiative transfer models

The Lyα emission line emerging from star-forming galaxies has been the subject of many studies over the last 40 yr, since the seminal paper by Partridge & Peebles (1967). Among more recent investigations, those by the Geneva group (see, for example, Schaerer 2007 which also includes a comprehensive set of references to earlier work) have focused in particular on the radiation transfer of Lyα photons in an expanding medium, in an attempt to reproduce the variety of Lyα profiles seen in high-redshift galaxies, where large-scale outflows are the norm. Having established the existence of such outflows in the Cosmic Horseshoe (Section 5.1), we can use the models by Verhamme et al. (2006) to interpret the Lyα profile in Fig. 7.

The basic idea is that the Lyα photons emitted from a central region of star formation, where the early-type stars and their H II regions are located, suffer multiple scatterings before they can escape the nebula. Such scatterings not only redistribute the photons in frequency, but also convert a fraction of them into IR photons if any dust is present. If the scattering medium is expanding, the net effect is a reduction of the Lyα luminosity (measured by the fraction, f_{esc}, of photons which manage to escape) and an overall shift of the wavelength distribution of the escaping photons to longer wavelengths, as blueshifted photons are absorbed by the H I gas in front of the stars. The profile of the emergent Lyα line (for a given SFR which determines the intrinsic Lyα luminosity) depends on a combination of parameters, principally the expansion velocity of the medium, v_{exp}; its internal velocity dispersion, normally measured by the parameter $b = \sqrt{2}\sigma$; the column density of neutral hydrogen, N(H I); and the column of dust, as measured by the colour excess $E(B - V)$.

The Lyα line in the Cosmic Horseshoe matches well some of the characteristics of the theoretical profiles generated by the Verhamme et al. (2006) models for the simplest geometrical configuration: a spherical shell expanding with uniform velocity. Indeed, as can be appreciated from Fig. 7 where the Lyα emission line and the Si II λ1526.7070 absorption line are plotted on a common velocity scale, the red wing of the former almost mirrors the blue wing of the latter, both extending to $|v| \simeq 700$–800 km s^{-1}. A prediction of the models is that there should be a maximum in the Lyα emission at a positive velocity (relative to the stars) $v = -2\, v_{\mathrm{exp}}$. In our case, the velocity of the longer wavelength peak, $v = +275$ km s^{-1} is indeed at about twice $|v| = 146$ km s^{-1} which we measured in Section 5.1 for the gas with the highest optical depth in absorption. Referring to fig. 12 of Verhamme et al. (2006), these are photons which have undergone just one backscattering from the receding portion of the expanding shell into our line of sight – with this frequency shift they can travel unabsorbed through the approaching (i.e. blueshifted) part of the shell. The long tail to $v \simeq 700$ km s^{-1} is made up of photons which have undergone two or more backscatterings, while the narrow component centred at $v = +115$ km s^{-1} consists of photons which have been multiply scattered from the approaching part of the shell.

The balance between the photons escaping from the approaching and receding portions of the shell – reflected in the relative flux of the two emission peaks – is a function of the column density of neutral hydrogen through the shell: as N(H I) increases, the more redshifted peak of emission dominates over the lower redshift one. Out of the illustrative examples considered by Verhamme et al. (2006) in their fig. 16, the case with $N(\mathrm{H\,I}) = 7 \times 10^{19}$ cm^{-2} matches our observed profile closely.

While this correspondence between simulated and observed profiles is impressive, other aspects of the models are less satisfactory. One of the difficulties in relating the Verhamme et al. (2006) models to our observations of the Cosmic Horseshoe stems from the fact that the absorption profiles of the interstellar lines do not fit the simple picture of an expanding shell with a well-defined velocity. With absorption extending over a thousand km s^{-1}, and without any information which would allow us to relate the velocity of the gas to its location within the galaxy, there is no obvious justification

for equating the velocity of the gas with the highest optical depth, $v = -146\,\mathrm{km\,s^{-1}}$, to the expansion velocity of the idealized shell. A further difficulty is that in the Verhamme et al. (2006) models there is also a strong dependence of the line profile on the velocity dispersion of the gas within the expanding shell. The clear distinction between the two redshifted peaks of emission requires not only low column densities of neutral gas [$N(\mathrm{H\,I}) \lesssim 5 \times 10^{20}\,\mathrm{cm^{-2}}$], but also relatively quiescent gas within the expanding shell ($|v_{\rm exp}|/b \gtrsim 5$). With the values we measure from the interstellar lines in the Horseshoe, $|v_{\rm exp}|/b = 145/105 \sim 1$, the profiles predicted by Verhamme et al. (2006) would look drastically different (see their fig. 15) and the two emission components would merge into one. The problem is exacerbated by the presence of gas at velocities as high as $v \simeq -800\,\mathrm{km\,s^{-1}}$ (see Fig. 4) which is not included in the models. A final point is that the models considered by Verhamme et al. (2006) generally assume unity covering factor of the central source of Lyα photons by the outflowing gas, whereas in the Cosmic Horseshoe the interstellar absorption lines appear to cover only ∼60 per cent of the stellar UV continuum (Section 5.2).

Presumably, the real geometrical configuration of stars, H II regions (which recall are at the same velocity as the stars – see Table 1), and outflowing ISM is more complicated than in the simple picture considered (for general illustrative purposes) by Verhamme et al. (2006). Treatments of Lyα radiation transfer in more complex situations have been examined in the literature, but generally with fewer specific realizations that can be compared directly to our observations of the Lyα line in the Cosmic Horseshoe. For example, Hansen & Oh (2006) considered the effects of a multiphase gas outflow, either in a shell with holes or in an ensemble of gas clumps. It is interesting that in their simulations the former scenario can still give a double-peak Lyα emission line, whereas the latter tends to generate more amorphous profiles. A further point of note is that in such multiphase outflows Lyα photons can escape even when the intervening column density of neutral hydrogen is high. It would obviously be of considerable interest to test whether a model tailored to the observed properties of the Cosmic Horseshoe can reproduce its Lyα profile.

6.3 Escape fraction of Lyα photons

Before concluding this section, we calculate the escape fraction of Lyα photons by comparing the observed Lyα luminosity with that of the UV continuum. In carrying out such a comparison, we convert the luminosities to SFRs using the conversions proposed by Kennicutt (1998), divided by a factor of 1.8 to account for the lower proportion of low-mass stars in the Chabrier (2003) IMF relative to the standard Salpeter (1955) IMF adopted by Kennicutt. We also correct for gravitational lensing magnification, although our conclusion is not sensitive to this factor, as we are comparing luminosities over the same regions of the Cosmic Horseshoe. In the lensing model by Dye et al. (2008), the magnification factor of the whole Einstein ring is 24; in Section 3 we calculated that the ESI slit captured a fraction 0.25 ± 0.05 of the total light. In the following, we do not carry the uncertainty in this estimate through the calculation, as it is the same for the Lyα line and the UV continuum, and we adopt a magnification factor of $24 \times 0.25 = 6$ for the portion of the Cosmic Horseshoe recorded with ESI. The comparison between SFR(Lyα) and SFR(UV) is sensitive to the reddening correction, since the two estimates are based on features at different wavelengths. We adopt $E(B-V) = 0.15$, as determined for the same two knots of the Horseshoe by Hainline et al. (2009 – see their discussion of the derivation of this value), together with the reddening curve of Calzetti et al. (2000).

From our ESI spectrum we measure a UV continuum luminosity at 1700 Å $L_\nu(1700\,\text{Å}) = 1.1 \times 10^{30}\,\mathrm{erg\,s^{-1}\,Hz^{-1}}$ which, using Kennicutt's (1998) conversion

$$\mathrm{SFR(UV)}(\mathrm{M_\odot\,yr^{-1}}) = 1.4 \times 10^{-28} L_\nu\,(\mathrm{erg\,s^{-1}\,Hz^{-1}}), \quad (4)$$

gives

$$\mathrm{SFR(UV)} = 159 \times 1/1.8 \times 3.8 \times 1/6 = 56\,\mathrm{M_\odot\,yr^{-1}} \quad (5)$$

with correction factors for the IMF, reddening and magnification, respectively.[1]

For comparison, Hainline et al. (2009) deduced $\mathrm{SFR(H}\alpha) = 113 \pm 17\,\mathrm{M_\odot\,yr^{-1}}$ from the Hα luminosity measured with NIRSPEC, but the comparison is complicated by the uncertainties in the respective flux calibrations. In any case, in galaxies at $z = 2$–3, there is an inherent dispersion (of about this magnitude) in star formation measurements from Hα emission and UV continuum (e.g. Pettini et al. 2001; Erb et al. 2006c) which can have a number of causes, apart from random errors. First, emission lines and UV continuum do not sample the same stellar populations: the luminosity of Hα is due primarily to the most massive stars, with shorter lifetimes than the wider range of stellar masses ($M \gtrsim 5\,\mathrm{M_\odot}$) whose integrated light makes up the continuum at 1700 Å. Second, the conversion from Hα (and Lyα) luminosity to SFR implicitly assumes that all the Lyman continuum (LyC) photons are absorbed within the H II region and reprocessed into emission lines – a situation which is often referred to as a 'radiation-bounded nebula'. Of course, if a fraction of LyC photons escape unabsorbed from the H II region, SFR(Hα) and SFR(Lyα) will be systematically lower than SFR(UV).

Turning to Lyα, we can use Kennicutt's (1998) calibration of SFR(Hα) and case B recombination to deduce

$$\mathrm{SFR(Ly}\alpha)(\mathrm{M_\odot\,yr^{-1}}) = 9.1 \times 10^{-43}\,L(\mathrm{Ly}\alpha)\,(\mathrm{erg\,s^{-1}}) \quad (6)$$

which, together with our measured $L(\mathrm{Ly}\alpha) = 2.0 \times 10^{43}\,\mathrm{erg\,s^{-1}}$, gives

$$\mathrm{SFR(Ly}\alpha) = 18 \times 1/1.8 \times 5.3 \times 1/6 = 8.9\,\mathrm{M_\odot\,yr^{-1}}, \quad (7)$$

where, as in equation (5), the correction factors account for the IMF, dust extinction and magnification, respectively.

By comparing the three estimates of SFR, we deduce $f_{\rm esc}^{\rm Ly\alpha} \simeq 0.16$–$0.08$, depending on whether we compare SFR(Lyα) to SFR(UV) or SFR(Hα), respectively. The former value is independent of the absolute flux calibration but assumes that, intrinsically (i.e. before the Lyα line is quenched by resonant scattering), SFR(UV) ≡ SFR(Lyα). Conversely, the latter value assumes no errors in the relative flux calibrations of the NIRSPEC and ESI data, and in the calculation of the fractions of the total light from the Horseshoe captured by the two spectrographs. However, either estimate of $f_{\rm esc}^{\rm Ly\alpha}$ is plausible, given the wide range found in other Lyα emitters (e.g. Pentericci et al. 2009; Verhamme et al. 2008). It must also be remembered that these values of $f_{\rm esc}^{\rm Ly\alpha}$ apply to our

[1] Recently, Leitherer (2008) re-examined Kennicutt's calibrations as given here in equations (4) and (6) in the light of new STARBURST99 models which include the effects of stellar rotation. While these models are still at an exploratory stage, the indications are that, at solar metallicities, they may result in ∼20 per cent reductions of the values of SFR deduced from both the UV continuum and Hα. At subsolar metallicities, however, SFR(Hα) is further reduced relative to SFR(UV), reflecting the harder ionizing spectrum of metal-poor massive stars. Such effects may partly explain why we deduce SFR(Hα) > SFR(UV) in the Cosmic Horseshoe.

viewing angle and to the area of the galaxy covered by the entrance slit of the spectrographs; the escape fraction could be higher in other directions (Neufeld 1991) and over larger areas (Saito et al. 2006).

Concluding this section, models of Lyα emission resonantly scattered by an expanding medium need further improvement in order to reproduce simultaneously the observed properties of the Lyα emission line and of the interstellar absorption lines in the Cosmic Horseshoe. Nevertheless, interpreting the Lyα line in terms of these models has given us some insight into the physical conditions of the gas. The main inference one would draw from the models of Verhamme et al. (2006) is that the column densities of neutral hydrogen and dust need to be relatively low – $N(\mathrm{H\,I}) \simeq 7 \times 10^{19}\,\mathrm{cm}^{-2}$ and $E(B-V) \simeq 0.1$ – in order for the line to exhibit two distinct emission peaks at the velocities observed. On the other hand, recall that in Section 5.2 we concluded that $\log N(\mathrm{H\,I})/\mathrm{cm}^{-2} \simeq 20.8$ *if* the first ions arise primarily in H I gas, as is the case in the Milky Way, damped Lyα systems, and the gravitationally lensed LBG cB58. The order of magnitude difference between these two estimates of the column density of gas can be reconciled if most of the gas in front of the stars in the Cosmic Horseshoe is ionized, with a neutral fraction of only about 10 per cent. The profile of the O I λ1302.1685 absorption line, which traces exclusively neutral gas, is consistent with this conclusion.

Given the sensitivity of the profile of the Lyα line to the geometrical and physical properties of the ambient interstellar medium, one may expect to see variations between even slightly different sightlines through the galaxy. In principle, the lensing magnification of the source offers a good opportunity to recognize such small-scale inhomogeneities. And yet no such variations are seen in the Cosmic Horseshoe. Recall (Section 3 and Fig. 1) that we obtained separate spectra for the two brightest knots in the Einstein ring, which we labelled 'Aperture 1' and 'Aperture 2'. After scaling the latter by a factor of 0.84 (derived empirically and found to be the same for the Lyα line and the UV continuum), the profiles of the Lyα line in the two apertures are identical within the limits of the noise, as can be appreciated from inspection of Fig. 8. Evidently, the same region of the source is lensed into the two knots of the Cosmic Horseshoe. This is all the more puzzling, given that Hainline et al. (2009) found that the ratio [N II] λ6584/Hα differs by almost a factor of 2 (at the $\sim 4\sigma$ significance level) between the two apertures. The [N II]/Hα ratio responds to changes in metallicity and ionization parameter (e.g. Kobulnicky & Kewley 2004; Pettini & Pagel 2004) which presumably are not the same in the regions of the galaxy lensed into Apertures 1 and 2 within the Einstein ring (knots 'A' and 'D' of Belokurov et al. 2007). Evidently, such variations do not have an impact on the Lyα emission morphology.

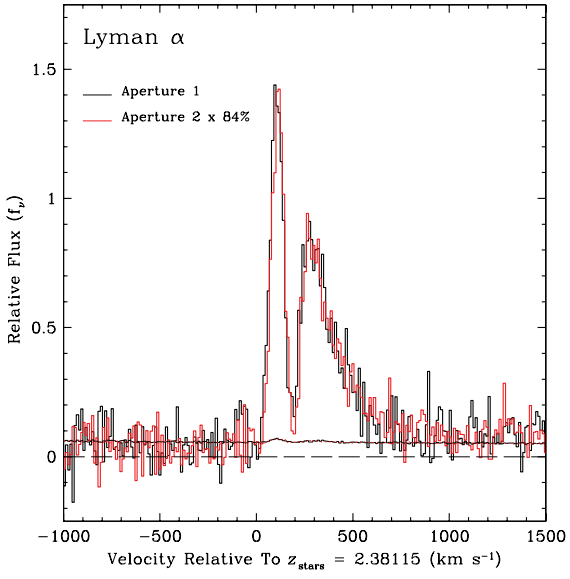

Figure 8. After scaling the flux in Aperture 2 (see Fig. 1) by a factor of 0.84, the Lyα profiles recorded from the two bright knots of emission in the Cosmic Horseshoe are indistinguishable from each other at the S/N of the present observations. The corresponding error spectra are also plotted (thin line near the zero level).

7 OTHER EMISSION LINES

The nebular C III] $\lambda\lambda$1906.683, 1908.734 doublet is clearly resolved in our ESI spectrum of the Cosmic Horseshoe (see Fig. 9). By fitting Gaussian profiles to the two lines, we deduced the parameters listed in Table 4. The mean redshift, $z_{\mathrm{C\,III]}} = 2.38115$, is in excellent agreement with the redshift of the OB stars, as expected (Section 4.1), and differs by only $-7\,\mathrm{km\,s}^{-1}$ from the weighted mean $\langle z_{\mathrm{H}\alpha}\rangle = 2.38123$ of the two apertures (see Fig. 1) measured separately by Hainline et al. (2009) from their NIRSPEC spectra. The good match attests to the mutual consistency of the ESI and NIRSPEC wavelength scales. The line widths are rather uncertain due to the limited S/N; with the prior condition that the width should be the same for both lines, we obtain $\sigma_{\mathrm{C\,III]}} = 62 \pm 7\,\mathrm{km\,s}^{-1}$ (this is the value used in the fits shown in Fig. 9), in very good agreement – again, as expected – with the weighted mean $\langle \sigma_{\mathrm{H}\alpha}\rangle = 65\,\mathrm{km\,s}^{-1}$ of the two apertures reported by Hainline et al. (2009).

As is well known, the ratio of these two C III] lines is a function of the electron density, varying from $F(1906)/F(1908) = 1.5$ to $\sim$0.8 in the range $n(e) = 100$–$30\,000\,\mathrm{cm}^{-3}$. Our measured $F(1906)/F(1908) = 1.1 \pm 0.2$ implies very high densities, in the range $n(e) \simeq 5000$–$25\,000\,\mathrm{cm}^{-3}$, which however may not be unusual for starbursts at $z = 2$–3 (Brinchmann, Pettini & Charlot 2008; Liu et al. 2008; Hainline et al. 2009).

We searched for nebular O III] $\lambda\lambda$1660.809, 1666.150 emission, but these lines are below the detection limit of our data. This is not surprising, given that the O III] doublet is weaker than C III] by a factor of $\sim$7 in the LBG composite spectrum of Shapley et al. (2003), and the C III] lines in the Cosmic Horseshoe are only detected at the $\sim 7\sigma$ significance level (Table 4). Any He II λ1640.418 emission from Wolf–Rayet stars is also too weak to be identified with certainty in our spectrum.

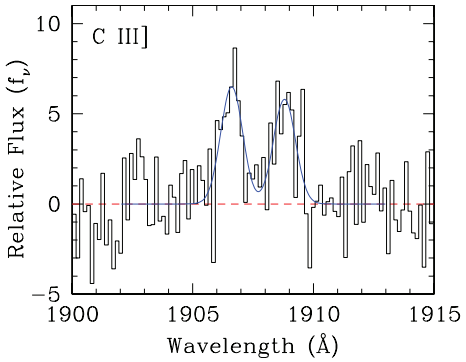

Figure 9. Histogram: portion of the ESI spectrum of the Cosmic Horseshoe in the region of the C III] $\lambda\lambda$1906.683, 1908.734 nebular emission lines, after subtracting the stellar continuum. Blue continuous line: Gaussian fits to the emission lines; see Table 4 and Section 7 for details.

Table 4. C III] emission lines.

Line	z	σ^a (km s^{-1})	F^b (10^{-18} erg s^{-1} cm^{-2})	L^b (10^{41} erg s^{-1})
1906.683	2.38103 ± 0.00014	62 ± 7	9.9 ± 1.3	1.29 ± 0.16
1908.734	2.38127 ± 0.00017	62 ± 7	8.8 ± 1.3	1.14 ± 0.16

[a]After correcting for the instrumental resolution ($\sigma_{\rm instr} = 32$ km s^{-1}), and constrained to be the same for both lines.
[b]Corrected for reddening and lensing magnification.

8 DISCUSSION

We now consider the results of the previous sections in the light of some of the questions raised in the Introduction.

8.1 Metallicity estimates

With available instrumentation, only strongly lensed galaxies offer the means to cross-check at high redshift the metallicity of early-type stars with that of the H II regions that surround them. We naturally expect the two measures to be the same, since the stars presumably formed very recently out of the gas which they now ionize; thus, this is essentially a consistency check between different metallicity indicators, all the more important given the known systematic offsets between different emission line measures of chemical abundance in H II regions (see, for example, Kewley & Ellison 2008). Such offsets in turn impact on the interpretation of chemical patterns and of trends, such as the mass–metallicity relation and its evolution with redshift, which can give us insights into galactic chemical evolution.

In Table 5 we have collected available determinations of element abundances in the Cosmic Horseshoe, bringing together the stellar data from Section 4 with the nebular measurements by Hainline et al. (2009). The first three entries in the table give the oxygen abundance deduced from strong emission line indices, respectively, the R23 index of Pagel et al. (1979), for which Hainline et al. (2009) used the calibration by Tremonti et al. (2004) based on observations of tens of thousands of nearby galaxies in the SDSS, and the N2 and O3N2 indices of Pettini & Pagel (2004). The last three entries in the table are from our analysis in this paper of UV spectral features from OB stars in the Horseshoe.

It is difficult to quote an error for each of the entries in Table 5; a realistic estimate should take into account the S/N of the data, the scatter in the adopted index calibration and the systematic bias which may affect it. However, most estimates evidently converge towards a metallicity of about a half solar (which, incidentally, is quite typical of star-forming galaxies at these redshifts – see Erb et al. 2006a). It is reassuring that stellar and nebular abundances are generally in good mutual agreement. The only deviant measure appears to be from the R23 method which is known, however, to overestimate the oxygen abundance in the near-solar regime, particularly when the calibration by Tremonti et al. (2004) is used (e.g. Kennicutt, Bresolin & Garnett 2003; Kewley & Ellison 2008).

Less satisfactory aspects of the comparison in Table 5 are (i) the poorly understood failure of the 1978 index of Rix et al. (2004) to provide a meaningful estimate of metallicity in this particular case; and (ii) the current limitations in the use of the wind lines as accurate abundance diagnostics. Point (i) can only be addressed with a larger set of high quality UV spectra of high-redshift galaxies. Until it is resolved, however, it may be unwise to use this index to investigate the possibility of a differential enrichment of Fe-peak elements compared to the products of Type II supernovae (Pettini et al. 2002; Halliday et al. 2008). Concerning point (ii), it is frustrating that while the strong wind lines are in principle one of the most easily measured abundance diagnostics – at least in data of sufficient resolution to resolve stellar and interstellar components – we still lack a comprehensive library of empirical UV spectra of OB stars of different metallicities to realize their full potential. The *HST* survey of the Magellanic Clouds by Leitherer et al. (2001) went some way towards remedying this situation, but their sampling of the upper H–R diagram is still too sparse to assemble separate sets of Large and Small Magellanic Cloud stars. The resulting hybrid library, obtained by combining all the available spectra into one set, can only give an approximate measure of metallicity, given the factor of $\sim$2 difference in the oxygen abundance of the two clouds.

Table 5. Metallicity comparison.

Method	Element(s)	$Z/Z^a_\odot$	Comments
R23	O	1.5	H II regions[b]
N2	O	0.5	H II regions[b]
O3N2	O	0.5	H II regions[b]
1425	C, Si, Fe	0.5	Photospheric, OB stars[c]
1978	Fe	...	Photospheric, B stars[c]
C IV	C, N, O, Fe	$\sim$0.6	Stellar wind, O stars[d]

[a]Abundance relative to solar (on a linear scale), using the compilation of solar abundances by Asplund, Grevesse & Sauval (2005).
[b]As reported by Hainline et al. (2009).
[c]This work (Section 4.2).
[d]This work (Section 4.3).

8.2 Escape of ionizing photons

It is still unclear what determines $f_{\rm esc}^{\rm LyC}$, the fraction of hydrogen ionizing photons which escape from star-forming galaxies into the IGM. Direct detection of these LyC photons has proved problematic until recently (e.g. Shapley et al. 2006; Iwata et al. 2009), and yet $f_{\rm esc}^{\rm LyC}$ must have been large at very high redshifts for the Universe to be re-ionized by the star formation activity thought to have taken place at $z > 6$ (e.g. Bolton & Haehnelt 2007; Ryan-Weber et al. 2009).

Observations of gravitationally lensed galaxies may offer insights into the factors that control $f_{\rm esc}^{\rm LyC}$. By fully resolving the interstellar absorption lines in our ESI spectrum of the Cosmic Horseshoe, we reached the conclusion that the interstellar gas only covers $\sim$60 per cent of the stellar UV light, as viewed from the Earth. This is a promising prerequisite for large values of $f_{\rm esc}^{\rm LyC}$, making the Horseshoe a high priority candidate in searches for LyC emission from high-z galaxies. On the other hand, if $\sim$40 per cent of the photons from the stars and surrounding H II regions really had a clear path out of the galaxy, we may have expected to see a strong

and narrow Lyα emission line centred at $z_{\rm H\,II}$, whereas no such feature is present in our spectrum. Possibly, some 40 per cent of the stars are located behind neutral gas of too low a column density to give discernible absorption in the metal lines, and yet capable of scattering most of the Lyα photons out of the line of sight (Hansen & Oh 2006). Whether such gas would be optically thick to LyC photons remains to be established.

Another necessary condition for the escape of LyC photons is a weaker Hα emission line than expected on the basis of the UV continuum luminosity and reddening (admittedly in the idealized case of continuous star formation at a constant rate). Such a disparity would arise from a 'matter-bounded nebula', where not all of the LyC photons emitted by the stars are absorbed and reprocessed within the H II region. As discussed in Section 6.3, in the Cosmic Horseshoe SFR(Hα) $\not\propto$ SFR(UV), although a number of different factors, apart from leakage of LyC photons, can affect this comparison. In conclusion, it would definitely be worthwhile to search for LyC emission in the Cosmic Horseshoe at wavelengths below 3085 Å (the redshifted value of the Lyman limit at $z = 2.38115$). Furthermore, it would be of interest to check for partial covering of the stars by the foreground interstellar medium in more galaxies among the newly discovered strongly lensed sources, ideally including galaxies with a range of Lyα equivalent widths. With such data in hand, we should be in a better position to understand the conditions that determine the escape fraction of LyC photons and the morphology of the Lyα line.

8.3 Comparison with MS 1512−cB58

One of the motivations for the present study was to establish how typical are the properties of the galaxy MS 1512−cB58, the only previous case where the gravitational lensing boost was sufficient to allow a detailed look at the spectrum of a high-redshift star-forming galaxy. While we have now doubled the 'sample' of high-z galaxies with good-quality ESI spectra, it would clearly be premature to draw general conclusions on the basis of just two objects. Nevertheless, one cannot help but being struck by how closely these two galaxies resemble each other in many of their properties. They are very similar in their overall metallicity and probably in their detailed chemical composition, indicating that they have reached comparable stages in the conversion of their gas reservoirs into stars. Their young stellar populations are largely indistinguishable in their UV spectral features, especially the P Cygni lines which are sensitive indicators of the mode of massive star formation and of differential reddening among stars at the upper end of the IMF. Most remarkable perhaps is the unexpected similarity in the properties of their outflowing interstellar media, with velocities spanning in both cases $\sim$1000 km s^{-1}, from -800 to $+250$ km s^{-1} relative to the stars, and involving comparable column densities of gas.

Presumably, it is just a coincidence that the first two galaxies at $z = 2$–3 whose UV spectra have been put under the 'microscope' of gravitational lensing have also turned out to be similar in so many respects. After all, we now know that the Cosmic Horseshoe and MS 1512−cB58 are also forming stars at comparable rates of $\sim$50–100 M$_\odot$ yr^{-1}, and have similar dynamical masses of $M_{\rm vir} \sim 1 \times 10^{10}$ M$_\odot$ (see Hainline et al. 2009 for these measurements in the Cosmic Horseshoe and Teplitz et al. 2000 for cB58). Future studies of other gravitationally lensed objects will arguably show a wider range of properties of star-forming galaxies at these redshifts.

What is interesting then, given the underlying similarity of the Horseshoe and cB58, is to consider the aspects in which they *differ*: the incomplete coverage of the stellar light by the interstellar absorption lines and the strikingly different Lyα morphologies. It is these two factors alone that would lead an observer to 'classify' the two galaxies differently. For example, in the rough breakdown of LBGs by Shapley et al. (2003) according to their UV spectral properties, cB58 would fall in the quartile with the highest interstellar absorption line equivalent widths and reddening, while the Cosmic Horseshoe would be in the quartile with the second highest Lyα *emission* equivalent width. And yet, from what we have uncovered in the present study, it may be the case that these differences are perhaps simply due to orientation effects – viewing two intrinsically similar galaxies along differing sightlines through their interstellar media, one (the Horseshoe) more rarefied and highly ionized than the other (cB58). With future studies of other strongly lensed galaxies we shall hopefully learn how to distinguish intrinsic differences from those caused by second-order effects, of which the direction from which we view the central starburst may be one example. For the moment, however, we must remain cautious of overinterpreting differences between different 'classes' of high-redshift galaxies, especially if such distinctions are based on the morphology and strength of the Lyα line, whose appearance is so sensitive to a variety of different parameters (e.g. Pentericci et al. 2009).

9 SUMMARY AND CONCLUSIONS

We have presented ESI observations of the rest-frame UV spectrum of a star-forming galaxy at $z = 2.38115$, lensed by a massive foreground galaxy into a nearly complete Einstein ring dubbed the 'Cosmic Horseshoe'. The high gravitational magnification affords the rare opportunity of recording the spectrum of this member of the $z = 2$–3 galaxy population at higher resolution and S/N than otherwise achievable, and thereby provides us with a close-up look of a galaxy during the epoch when cosmic star formation activity was at its peak. Our main findings are as follows.

(i) The Cosmic Horseshoe shares many of its properties with the population of 'BX' galaxies selected with the colour criteria of Steidel et al. (2004). Its metallicity $Z \simeq 0.5\,Z_\odot$, dynamical mass $M_{\rm vir} \simeq 1 \times 10^{10}$ M$_\odot$ and reddening $E(B-V) = 0.15$ are all typical of those galaxies (Erb et al. 2006a,b,c). With a SFR $\simeq 100$ M$_\odot$ yr^{-1}, the Horseshoe is among the most luminous galaxies in the BX sample.

(ii) Generally, there is good agreement between different metallicity indicators based, respectively, on ratios of strong nebular emission lines, on blends of stellar photospheric lines and on P Cygni lines from the most luminous OB stars. The R23 index of Pagel et al. (1979) seems to overpredict the oxygen abundance by a factor of $\sim$3, when calibrated with the prescription by Tremonti et al. (2004). Of the stellar measures, the 1978 index of Rix et al. (2004) does not fit the data well due to excess absorption not present in the models and whose identity remains unclear.

(iii) A continuous mode of star formation with a Salpeter slope for stars with masses $100 \geq M \geq 5$ M$_\odot$ gives a good representation of the UV spectrum; we see no evidence for a departure from a Salpeter IMF, nor differential reddening among massive stars, in the contrast of the P Cygni lines over the underlying UV continuum.

(iv) The interstellar absorption lines are broad, extending over a velocity interval of $\sim$1000 km s^{-1}, from -800 to $+250$ km s^{-1} relative to the redshift of the stars and H II regions. The gas with the highest optical depths is outflowing from the regions of star formation with a speed of $\sim$150 km s^{-1}, and only covers $\sim$60 per cent of the stellar continuum light.

(v) The Lyα line is in emission and shares many of the properties of the so-called Lyα emitters, although its equivalent width is a factor of $\sim$2 smaller than the lower limit $W_0(\mathrm{Ly}\alpha) \geq 20$ Å commonly adopted to define this subset of galaxies. The resolved line profile matches well those computed with models of resonantly scattered Lyα photons in an expanding medium, although such models find it difficult to account for the fact that the velocity dispersion of the gas is comparable to its bulk expansion velocity, and for the existence of gas extending over hundreds of km s^{-1} in velocity space. Some $\sim$10–15 per cent of the Lyα photons produced escape the galaxy, the remainder presumably being absorbed by dust and recycled into IR photons, or scattered over a larger area than that covered by our narrow-slit observations. It remains to be established what fraction of the Lyman *continuum* photons emitted by the stars leak into the IGM.

(vi) Overall, many of the physical properties of the stars and interstellar medium of the Cosmic Horseshoe are similar to those of the only other galaxy previously studied at comparable resolution and S/N, MS 1512−cB58 at $z = 2.7276$. This may not be surprising, given that both galaxies are fairly typical examples of the star-forming galaxy population at these redshifts. The fundamental similarities between the two objects highlight the fact that the aspects in which they differ, particularly the very different morphologies of their Lyα lines, may be due to superficial reasons, such as differing viewing angles, rather than to more deeply rooted causes.

In the near future it should be possible to make further progress on all of these topics with the increasing numbers of strongly lensed high-redshift galaxies being discovered by the SDSS and other lensing surveys.

ACKNOWLEDGMENTS

We are grateful to the staff at the W. M. Keck Observatory for their competent assistance with the observations, to Sam Rix and Dan Nestor who generously provided some of the software used in the analysis of the spectra and to Simon Dye for clarifications concerning the lensing models. Lindsay King kindly allowed us to reproduce her ESO/FORS2 image of the Cosmic Horseshoe in Fig. 1. We also thank the anonymous referee for helpful comments which have improved the paper. AMQ's research is funded by a scholarship from the Marshall Foundation. AES acknowledges support from the David and Lucile Packard Foundation and the Alfred P. Sloan Foundation, and CCS acknowledges support from NSF grant AST-0606912 and the John D. and Catherine T. MacArthur Foundation. Finally, we wish to extend thanks to those of Hawaiian ancestry on whose mountain we are privileged to be guests.

REFERENCES

Asplund M., Grevesse N., Sauval A. J., 2005, in Barnes T. G., III, Bash F. N., eds, ASP Conf. Ser. Vol. 336, Cosmic Abundances as Records of Stellar Evolution and Nucleosynthesis. Astron. Soc. Pac., San Francisco, p. 25
Baker A. J., Lutz D., Genzel R., Tacconi L. J., Lehnert M. D., 2001, A&A, 372, L37
Baker A. J., Tacconi L. J., Genzel R., Lehnert M. D., Lutz D., 2004, ApJ, 604, 125
Belokurov V. et al., 2007, ApJ, 671, L9
Belokurov V., Evans N. W., Hewett P. C., Moiseev A., McMahon R. G., Sanchez S. F., King L. J., 2009, MNRAS, 392, 104
Bolton J. S., Haehnelt M. G., 2007, MNRAS, 382, 325
Brinchmann J., Pettini M., Charlot S., 2008, MNRAS, 385, 769
Calzetti D., Armus L., Bohlin R. C., Kinney A. L., Koornneef J., Storchi-Bergmann T., 2000, ApJ, 533, 682
Chabrier G., 2003, PASP, 115, 763
Chandar R., Leitherer C., Tremonti C. A., Calzetti D., Aloisi A., Meurer G. R., de Mello D., 2005, ApJ, 628, 210
Crowther P. A., Prinja R. K., Pettini M., Steidel C. C., 2006, MNRAS, 368, 895
Dye S., Evans N. W., Belokurov V., Warren S. J., Hewett P., 2008, MNRAS, 388, 384
Ellingson E., Yee H. K. C., Bechtold J., Elston R., 1996, ApJ, 466, L71
Erb D. K., Shapley A. E., Pettini M., Steidel C. C., Reddy N. A., Adelberger K. L., 2006a, ApJ, 644, 813
Erb D. K., Steidel C. C., Shapley A. E., Pettini M., Reddy N. A., Adelberger K. L., 2006b, ApJ, 646, 107
Erb D. K., Steidel C. C., Shapley A. E., Pettini M., Reddy N. A., Adelberger K. L., 2006c, ApJ, 647, 128
Faucher-Giguère C.-A., Lidz A., Hernquist L., Zaldarriaga M., 2008, ApJ, 682, L9
Finkelstein S. L., Papovich C., Rudnick G., Egami E., Le Floc'h E., Rieke M. J., Rigby J. R., Willmer C. N. A., 2009, ApJ, 700, 376
Grimes J. P. et al., 2009, ApJS, 181, 272
Hainline K. N., Shapley A. E., Kornei K. A., Pettini M., Buckley-Geer E., Allam S. S., Tucker D. L. 2009, ApJ, accepted (arXiv:0906.2197)
Halliday C. et al., 2008, A&A, 479, 417
Hansen M., Oh S. P., 2006, MNRAS, 367, 979
Heckman T. M., Lehnert M. D., Strickland D. K., Armus L., 2000, ApJS, 129, 493
Hu E. M., Cowie L. L., McMahon R. G., 1998, ApJ, 502, L99
Iwata I. et al., 2009, ApJ, 692, 1287
Jenkins E. B., Tripp T. M., 2006, ApJ, 637, 548
Kennicutt R. C, Jr., 1998, ARA&A, 36, 189
Kennicutt R. C, Jr., Bresolin F., Garnett D. R., 2003, ApJ, 591, 801
Kewley L. J., Ellison S. L., 2008, ApJ, 681, 1183
Kobulnicky H. A., Kewley L. J., 2004, ApJ, 617, 240
Kubo J. M., Allam S. S., Annis J., Buckley-Geer E. J., Diehl H. T., Kubik D., Lin H., Tucker D., 2009, ApJL, 696, L61
Kudritzki R.-P., Puls J., 2000, ARA&A, 38, 613
Leitherer C., 2008, in Hunt K. L., Madden S., Schneider R., eds, IAU Symp. 255, Low-Metallicity Star Formation: From the First Stars to Dwarf Galaxies. Cambridge Univ. Press, Cambridge, p. 305
Leitherer C. et al., 1999, ApJS, 123, 3
Leitherer C., Leão J. R. S., Heckman T. M., Lennon D. J., Pettini M., Robert C., 2001, ApJ, 550, 724
Leitherer C., Calzetti D., Martins L. P., 2002, ApJ, 574, 114
Liu X., Shapley A. E., Coil A. L., Brinchmann J., Ma C.-P., 2008, ApJ, 678, 758
Mar D. P., Bailey G., 1995, Publ. Astron. Soc. Aust., 12, 239
Martin C. L., 2005, ApJ, 621, 227
Martin C. L., Bouché N., 2009, ApJ, submitted
Mas-Hesse J. M., Kunth D., Tenorio-Tagle G., Leitherer C., Terlevich R. J., Terlevich E., 2003, ApJ, 598, 858
Morton D. C., 2003, ApJS, 149, 205
Neufeld D. A., 1991, ApJ, 370, L85
Pagel B. E. J., 2003, in Charbonnel C., Schaerer D., Meynet G., eds, ASP Conf. Ser. Vol. 304, CNO Abundances in Dwarf and Spiral Galaxies. Astron. Soc. Pac., San Francisco, p. 187
Pagel B. E. J., Edmunds M. G., Blackwell D. E., Chun M. S., Smith G., 1979, MNRAS, 189, 95
Papovich C., Dickinson M., Ferguson H. C., 2001, ApJ, 559, 620
Partridge R. B., Peebles P. J. E., 1967, ApJ, 147, 868
Pentericci L., Grazian A., Fontana A., Castellano M., Giallongo E., Salinbeni S., Santini P., 2009, A&A, 494, 553
Pettini M., 2006, in LeBrun V., Mazure A., Arnouts S., Burgarella D., eds, The Fabulous Destiny of Galaxies: Bridging Past and Present. Frontier Group, Paris, p. 319
Pettini M., Pagel B. E. J., 2004, MNRAS, 348, L59
Pettini M., Steidel C. C., Adelberger K. L., Dickinson M., Giavalisco M., 2000, ApJ, 528, 96

Pettini M., Shapley A. E., Steidel C. C., Cuby J.-G., Dickinson M., Moorwood A. F. M., Adelberger K. L., Giavalisco M., 2001, ApJ, 554, 981
Pettini M., Rix S. A., Steidel C. C., Adelberger K. L., Hunt M. P., Shapley A. E., 2002, ApJ, 569, 742
Pettini M. et al., 2007, Nuovo Cimento B, 122, 1043
Reddy N. A., Steidel C. C., 2009, ApJ, 692, 778
Reddy N. A., Steidel C. C., Pettini M., Adelberger K. L., Shapley A. E., Erb D. K., Dickinson M., 2008, ApJS, 175, 48
Rhoads J. E., Malhotra S., Dey A., Stern D., Spinrad H., Jannuzi B. T., 2000, ApJ, 545, L85
Rix S. A., Pettini M., Leitherer C., Bresolin F., Kudritzki R.-P., Steidel C. C., 2004, ApJ, 615, 98
Ryan-Weber E. V., Pettini M., Madau P., Zych B. J., 2009, MNRAS, 395, 1476
Saito T., Shimasaku K., Okamura S., Ouchi M., Akiyama M., Yoshida M., 2006, ApJ, 648, 54
Salpeter E. E., 1955, ApJ, 121, 161
Savage B. D., Sembach K. R., 1991, ApJ, 379, 245
Savaglio S., Panagia N., Padovani P., 2002, ApJ, 567, 702
Sawicki M., 2001, AJ, 121, 2405
Schaerer D., 2009, in Cepa J., ed., The Emission Line Universe. Cambridge Univ. Press, Cambridge, p. 106
Seitz S., Saglia R. P., Bender R., Hopp U., Belloni P., Ziegler B., 1998, MNRAS, 298, 945
Shapley A. E., Steidel C. C., Adelberger K. L., Dickinson M., Giavalisco M., Pettini M., 2001, ApJ, 562, 95
Shapley A. E., Steidel C. C., Pettini M., Adelberger K. L., 2003, ApJ, 588, 65
Shapley A. E., Steidel C. C., Erb D. K., Reddy N. A., Adelberger K. L., Pettini M., Barmby P., Huang J., 2005, ApJ, 626, 698
Shapley A. E., Steidel C. C., Pettini M., Adelberger K. L., Erb D. K., 2006, ApJ, 651, 688
Sheinis A. I., Miller J. S., Bolte M., Sutin B. M., 2000, Proc. SPIE, 4008, 522
Siana B., Teplitz H. I., Chary R.-R., Colbert J., Frayer D. T., 2008, ApJ, 689, 59
Smail I. et al., 2007, ApJ, 654, L33
Stark D. P., Swinbank A. M., Ellis R. S., Dye S., Smail I. R., Richard J., 2008, Nat, 455, 775
Steidel C. C., Adelberger K. L., Giavalisco M., Dickinson M., Pettini M., 1999, ApJ, 519, 1
Steidel C. C., Shapley A. E., Pettini M., Adelberger K. L., Erb D. K., Reddy N. A., Hunt M. P., 2004, ApJ, 604, 534
Tapken C., Appenzeller I., Noll S., Richling S., Heidt J., Meinköhn E., Mehlert D., 2007, A&A, 467, 63
Teplitz H. I. et al., 2000, ApJ, 533, L65
Tremonti C. A. et al., 2004, ApJ, 613, 898
Vanzella E. et al., 2009, ApJ, 695, 1163
Verhamme A., Schaerer D., Maselli A., 2006, A&A, 460, 397
Verhamme A., Schaerer D., Atek H., Tapken C., 2008, A&A, 491, 89
Wilkins S. M., Hopkins A. M., Trentham N., Tojeiro R., 2008, MNRAS, 391, 363
Yee H. K. C., Ellingson E., Bechtold J., Carlberg R. G., Cuillandre J.-C., 1996, AJ, 111, 1783
Yuan T.-T., Kewley L. J., 2009, ApJL, 699, L161

This paper has been typeset from a TEX/LATEX file prepared by the author.